Numerical study of Ar/CF$_4$/N$_2$ discharges in single- and dual-frequency capacitively coupled plasma reactors

V. Georgieva,[a] A. Bogaerts, and R. Gijbels
Department of Chemistry, University of Antwerp (UIA), Universiteitsplein 1,
B-2610 Wilrijk-Antwerp, Belgium

A one-dimensional particle-in-cell/Monte Carlo model is developed to study capacitively coupled (cc) radio-frequency discharges in a gas mixture of Ar, CF$_4$, and N$_2$. The charged species, which are followed in the model, are: Electrons and Ar$^+$, CF$_3^+$, N$_2^+$, F$^-$, and CF$_3^-$ ions. The simulation considers electron – neutral (Ar, CF$_4$, and N$_2$) collisions, various kinds of collisions of ions with neutrals, positive–negative ion recombination, and electron–ion recombination. The model yields results for electron and ion densities, fluxes and energy distributions, collision rates and electric field, and potential distributions. The simulations are performed for a 0.8/0.1/0.1 ratio of Ar/CF$_4$/N$_2$ mixture at a pressure of 30 mTorr in single (13.56 MHz) and dual frequency (2 + 27 MHz) cc reactors and a comparison between the two frequency regimes is made. Results show that the structure of the discharges is electronegative in both cases. F$^-$ and CF$_3^-$ ions are the main negative charge carriers in the single and dual frequency regime, respectively. In the presence of low-frequency (2 MHz) and a strong electric field, the light F$^-$ ions are no longer confined in the bulk plasma and they partially respond to the instantaneous electric field. The calculated electron energy probability function profiles can be approximated to a Druyvesteyn and bi-Maxwellian distribution with high-energy tails in the single- and dual-frequency regime, respectively. The ion energy distribution is narrow with one outstanding peak in the single-frequency scheme, whereas it is wide and bimodal in the dual-frequency scheme. © *2003 American Institute of Physics.* [DOI: 10.1063/1.1603348]

I. INTRODUCTION

Radio-frequency (rf) plasma etching is well recognized for its anisotropy, which is a critical process parameter in integrated circuit manufacturing. Conventional capacitively coupled (cc) reactors powered by 13.56 MHz rf sources meet many plasma processing requirements. However, the scaling evolution of semiconductor devices needs more and more accurate transfer patterns with minimum damage on the substrate, which can be achieved by the precise control of both the ion bombardment energy and the ion flux. Single-frequency systems face difficulties providing an independent control of ion energy. For that purpose, dual-frequency systems have been introduced and studied.[1–7] The dual rf excitation setup allows the plasma density to be determined by one high-frequency (HF), e.g., 13.56 or 27 MHz, or very high-frequency (VHF) source, e.g., 100 MHz, while the substrate self-bias voltage is controlled by the secondary low-frequency (LF), e.g., in the order of 1 MHz.[2–7] In addition, the LF–(V)HF scheme provides a significantly wider ion bombardment energy range in comparison with a single-HF configuration.[1–7] Therefore, the study of this plasma processing is of great importance for further improvement of its performance. In the early 90's, Goto *et al.*[1] introduced the cc HF–VHF (13.56 – 100 MHz) setup and demonstrated its advantages in low ion energy etching. The discharge was maintained between two electrodes, one of them was driven

by a VHF power supply and the other biased by HF. The wafer was placed on the biased electrode. Later on, other dual-frequency schemes, like LF–(V)HF and commensurate frequencies, were applied.[2–6] Tsai *et al.*[2] experimentally investigated etching of SiO$_2$ structures in a dual-frequency (27/2 MHz) Ar/CO/CF$_x$ discharge. The dependence of plasma parameters on the substrate frequency and power has also been numerically studied by particle-in-cell (PIC)[3] and fluid[4] models. It was shown that the plasma density is predominantly determined by the primary power source while self-bias and ion bombardment energy are determined by the substrate power source.[3,4] The experimental study of Ar and Ar/CF$_4$ plasma structures in LF–(V)HF reactors demonstrated that LF biasing and HF plasma production could be functionally separated by increasing the sustaining frequency from 13.56 MHz (HF) to 100 MHz (VHF).[5] However, if the source frequencies are close to each other (e.g., 6.78 and 13.56 MHz) the nonlinear interaction effects can be strong and the resulting plasma characteristics cannot be independently controlled.[6] Recently, an Ar/CF$_4$ discharge has been numerically investigated in a pulsed LF–VHF reactor.[7] The reduction of the local charging by allowing negative ions to reach the electrodes during the off phase has been discussed. The simulation results of the present work show that the same effect can be achieved by applying a different dual-frequency configuration. In the present reactor, the two power supplies are both applied to one of the electrodes and the other electrode is grounded. The wafer is placed on the driven electrode. The purpose of the present work is to study

---

[a]Electronic mail: vgeorg@uia.ua.ac.be

3748

J. Appl. Phys., Vol. 94, No. 6, 15 September 2003
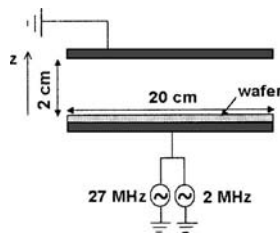
Georgieva, Bogaerts, and Gijbels   3749

FIG. 1. Schematic diagram of the dual-frequency reactor.

numerically, the discharge structure and properties, and to compare the simulation results of the plasma parameters in a conventional cc single-frequency (13.56 MHz) and dual-frequency $(2+27\,\text{MHz})$ reactor by means of a one-dimensional PIC/Monte Carlo (MC) method. The influence of the second LF on the discharge parameters, such as charged particle densities and energy distributions, is discussed.

Plasma chemical issues are as much important in the further optimization of etching processes as plasma processing units. Feedgas mixes are usually complex because of the conflicting requirements on the etch rate, selectivity to mask, and anisotropy. Carbon tetrafluoride (CF_4) is a basic component in gas mixtures for plasma etching of silicon and silicon dioxide and, therefore, is the most well-studied etch system (e.g., Refs. 1 and 8–11). While the investigation of pure CF_4 discharges gives the pattern for describing plasma etching, the study of discharges in a mixture of Ar and CF_4, which is often used for etching, provides insight into the process.[5,7,12,13]

In our previous paper, we presented a one-dimensional PIC/MC model and clarified the plasma structure and parameters in electropositive Ar, electronegative CF_4, and Ar/CF_4 discharges at different ratios.[12] A rapid decrease in electron density is observed with the addition of even a small amount of CF_4 to Ar, i.e., the dominant negative charge carriers are the negative ions, and this profoundly influences the sheath dynamics. In the present article, the model is extended to examine the discharge structure in a mixture of Ar, CF_4, and N_2, which is a feedstock gas for etching in industrial cc dual-frequency reactors.

In Sec. II, the input parameters, the outline of the model, and the collisions included in the simulation are given. In Sec. III, the results of the simulation, such as the electric field and potential distributions, charged particle densities, and energy distributions, are presented and discussed. Finally, in Sec. IV, a summary is given.

II. DESCRIPTION OF THE MODEL

A schematic diagram of the dual-frequency cc reactor considered in this study is shown in Fig. 1. The plasma is sustained between two parallel plates, each is 20 cm in diameter and separated from the other by 2 cm. One of the electrodes is driven by a single- (13.56 MHz) or dual-frequency $(2+27\,\text{MHz})$ power source. The amplitude of the applied voltage is 700 V. The other electrode is grounded. The simulation is carried out at a pressure of 30 mTorr. It should, however, be mentioned that the model presented

here, can also be applied to other discharge conditions. The computation is based on a one-dimensional coordinate space and three-dimensional velocity space PIC/MC algorithm. The motion of the charged particles is simulated by the PIC method using the standard explicit "leap frog" finite difference scheme. A PIC simulation treats the charged particles in a kinetic way. It is attractive because the fields and the energy distributions are obtained self-consistently from first principles.[14] The collisions between the charged particles are added by combining the PIC model with a MC procedure. In the case of modeling of electronegative discharges, the major disadvantage of this method is that it requires a long computational time to reach convergence. The negative charges are confined in the bulk plasma and the only loss mechanism, i.e., ion–ion recombination, has a relatively low reaction frequency. Kawamura et al.[15] point out many physical and numerical methods of speeding up the PIC calculations. Some of the methods, such as longer ion time steps, different weights for electrons and ions, and improved initial density profiles, are applied in this simulation. A more detailed description of the PIC technique can be found in Birdsall and Langdon.[14] Electrons are absorbed and ions are neutralized on the electrodes. Secondary electron emission is included here because the rf discharge is assumed to be in the γ-regime at the conditions under study.[16,17] The initial densities of the charged species in the model are based on experimental and simulation data;[8–13] the initial velocities are calculated from the Maxwellian distribution at an average electron temperature of 2 eV and an average ion temperature of 0.043 eV (500 K).[18]

The charged species, which are followed in the model, are: Electrons, Ar^+, CF_3^+, N_2^+, F^-, and CF_3^- ions. Simulation results in a pure cc rf CF_4 discharge show that the dominant positive ions are CF_3^+, with a density exceeding those of CF_2^+, CF^+, C^+, and F^+ by more than 2 to 3 orders of magnitude, and $N_{CF_{3+}} \cong N_{F-} + N_{CF_{3-}} + N_e$, where N denotes the number densities in the bulk plasma.[11] For that reason, CF_3^+ is the only type of positive ions of CF_4 followed in the model.

The interactions between the particles are treated by the MC method, which is basically a probabilistic approach. To calculate collision probabilities, it is necessary to have the corresponding collision cross section data, which are not always available. Hence, the present model uses several techniques to define the collision probabilities even when the collision cross sections are unknown.

The electron – neutral collision probability is determined by the null collision method based on cross section data.[19] In the present model, however, the expression for determining the electron scattering angle differs from the one proposed in Ref. 19, as is explained in Ref. 20. The Ar^+ $-Ar$, Ar^+-N_2, $N_2^+-N_2$, and N_2^+-Ar collision probabilities are calculated in the same way. The other ion – neutral elastic and reactive collisions, included in the model, are calculated by an ion–molecule collision model for endothermic reactions.[11] The positive–negative ion recombination probability is determined from a recombination rate constant.[21] The outlines of all techniques are given in our previous paper.[12] In this article, the electron – positive ion

3750   J. Appl. Phys., Vol. 94, No. 6, 15 September 2003

Georgieva, Bogaerts, and Gijbels

TABLE I. Electron–neutral (Ar, CF$_4$, and N$_2$) collisions taken into account in the model.

Reaction	ε_{th} (eV)	Reference No.
$e + Ar \rightarrow e + Ar$	...	22
$e + Ar \rightarrow e + Ar^*$	11.5	22
$e + Ar \rightarrow 2e + Ar^+$	15.8	22
$e + N_2 \rightarrow e + N_2^*(Y)^a$	...	23
$e + N_2 \rightarrow 2e + N_2^+(Y)^b$	15.6	23
$e + N_2 \rightarrow 2e + N_2^+(B^2\Sigma)$	18.8	23
$e + CF_4 \rightarrow e + CF_4$	...	24
$e + CF_4 \rightarrow e + CF_4(v1)$	0.108	24
$e + CF_4 \rightarrow e + CF_4(v3)$	0.168	24
$e + CF_4 \rightarrow e + CF_4(v4)$	0.077	24
$e + CF_4 \rightarrow e + CF_4^*$	7.54	24
$e + CF_4 \rightarrow F^- + CF_3$	6.4	24
$e + CF_4 \rightarrow F + CF_3^-$	5	25
$e + CF_4 \rightarrow e + F^- + CF_3^+$	12	25
$e + CF_4 \rightarrow 2e + F + CF_3^+$	16	24
$e + CF_4 \rightarrow e + F + CF_3$	12	24
$e + CF_4 \rightarrow e + 2F + CF_2$	17	24
$e + CF_4 \rightarrow e + 3F + CF$	18	24

[a] N2 (Y) = N$_2(\nu = 0-8, A\,^3\Sigma, B\,^3\Pi, W\,^3\Delta, B'\,^3\Sigma, a'\,^1\Sigma, a'\,^1\Pi, w\,^1\Delta,$ $C\,^3\Pi, E\,^3\Sigma, a''\,^1\Sigma,$ and "sum of singlets," including dissociation).
[b] N$_2^+$(Y) = N$_2^+$ ($X\,^2\Sigma$ and $A\,^2\Pi$).

TABLE II. Positive–negative ion and electron–positive ion recombination reactions considered in the model and the corresponding recombination rate coefficients.

Reaction	Rate constant (m^3/s)	Reference No.
$F^- + Ar^+ \rightarrow F + Ar$	1.0×10^{-13}	29
$F^- + CF_3^+ \rightarrow F + CF_3$	1.0×10^{-13}	29
$CF_3^- + Ar^+ \rightarrow CF_3 + Ar$	1.0×10^{-13}	29
$CF_3^- + CF_3^+ \rightarrow CF_3 + CF_3$	1.0×10^{-13}	29
$e + CF_3^+ \rightarrow CF_3$	$3.95 \times 10^{-15}/\sqrt{T_e}T_i$	30
$e + N_2^+ \rightarrow 2N(^4S)$	$4.8 \times 10^{-13}\sqrt{300/T_e(K)}$	31

the radical species on plasma characteristics in the near future.

The Ar$^+$ − Ar and N$_2^+$ − N$_2$ elastic isotropic and backward scattering (to simulate charge transfer) cross sections are taken from Phelps.[27] The cross section data for nonresonant charge transfer between Ar$^+$ and N$_2$, and between N$_2^+$ and Ar are adopted from Spalburg and Gislason.[28] The collision probabilities for these reactions are calculated by the null-collision method.[19]

The CF$_3^+$ − CF$_4$, F$^-$ − CF$_4$, and CF$_3^-$ − CF$_4$ elastic and reactive collisions are simulated using the ion–molecule collision model for endothermic reactions developed by Nanbu and Denpoh.[11] A complete overview of the ion − CF$_4$ reactions considered in the model (127 in total) and of the corresponding thermodynamic threshold energies, is given in Ref. 12. The Ar$^+$ − CF$_4$, CF$_3^+$ − Ar, F$^-$ − Ar, and CF$_3^-$ − Ar elastic collisions are treated by means of the same technique.[12]

The positive–negative ion and electron − ion recombination reactions, the corresponding rate constants, and the references, are presented in Table II. The ion–ion and electron–ion recombination cross sections and, hence, the probabilities are determined from a given expression for the corresponding rate constant, as proposed by Nanbu and Denpoh.[21,30] We have already explained the collision model for ion − ion recombination.[12] The dependence of the electron − ion recombination rate constants on the electron temperature T_e and ion temperature T_i makes the model more complicated. The electron − ion recombination is treated using the null-collision technique.[30] Let us express the electron − ion rate constants as $k_{e-i} = a/(T_e)^{1/2}$, where a is equal to $3.95 \times 10^{-15}/Ti$ and 7.72×10^{-14} for electron − CF$_3^+$ and electron − N$_2^+$ recombination, respectively. The electron temperature is calculated from $T_e = m_e \nu_e^2/3e$, where m_e and ν_e are the mass and velocity of the electron, respectively, and e is the electron charge. The probability that an electron with velocity ν_e recombines with a positive ion in time step Δt is given by[30]

$$P_{r_{e-i}} = W_i \frac{N_i}{V_c} \frac{a}{\sqrt{m_e/3e}} \frac{\Delta t}{\nu_e}, \qquad (1)$$

where W_i and N_i are the ion weight (representing the real number of ions in one simulated superparticle) and the number of the simulated ions, respectively, in a cell with a volume V_c. Since Eq. (1) has a singularity at $\nu_e = 0$, a cutoff parameter $(\nu_e)_{min}$ is introduced to obtain the maximum re-

(CF_3^+ and N_2^+) recombination is included and details for the method are given later in this section.

The electron–neutral (Ar, CF$_4$, and N$_2$) collisions considered in this simulation, along with the corresponding threshold energies and references, are presented in Table I. The collisions of electrons with other neutrals, like CF$_4$ radicals (CF$_3$, CF$_2$, CF, and F), excited states of N$_2$, and atomic nitrogen can significantly influence the ion and electron densities, and electron temperature, depending on the power, pressure, flow rate, etc. The present model does not take into account these collisions and the approximation is reasonable based on the following considerations. The computational and experimental results in a pure CF$_4$ discharge show that the densities of the radicals at low pressure are much lower in comparison with the CF$_4$ density, with values in the order of 10^{18} m^{-3}.[9,10] An experimental investigation of dc magnetron Ar/N$_2$ discharges at a pressure of 25 mTorr demonstrates that the atomic nitrogen equals between 0.13% and 0.24% of the molecular nitrogen depending on the fractional N$_2$ concentration.[26] Consequently, in the investigated gas mixture, which consists of 80% Ar, 10% CF$_4$, and 10% N$_2$, and at low pressure (30 mTorr), the concentration and collision frequency of the other neutrals with the electrons are expected to be much smaller than the concentration and the collision frequency of the background gas neutrals with the electrons. In addition, in comparison with the PIC/MC method, a fluid model is more suitable to follow the radicals and excited states, since the PIC/MC method assumes that the background gas neutrals are distributed uniformly in the discharge, which is not applicable to the other neutral species (e.g., see the space distributions of CF and CF$_2$ presented in Ref. 10). Recently, a fluid model to study pure CF$_4$ discharges has been developed by our group. We will compare the results from the two models and present the influence of
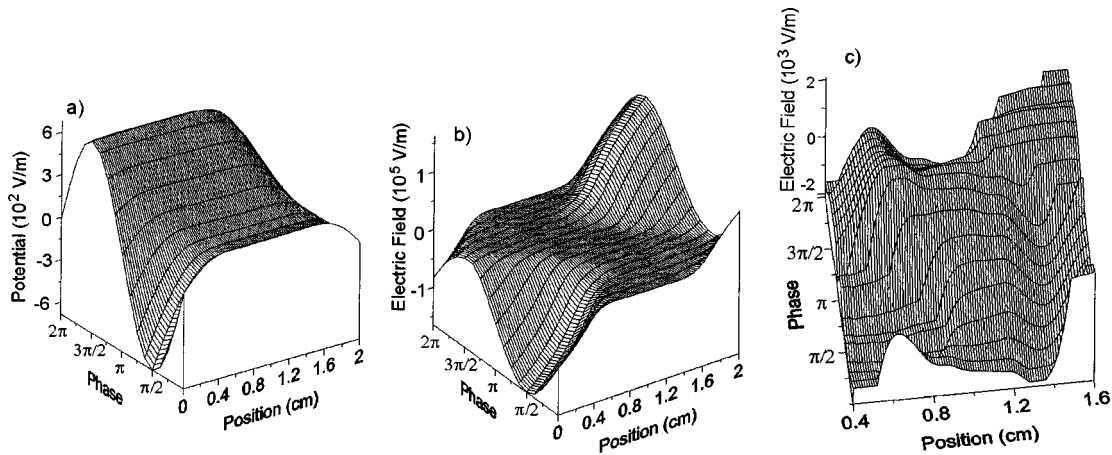
FIG. 2. Potential distribution (a) and electric-field distributions in the entire discharge (b), and in the bulk region (c), as a function of time in the HF (13.56 MHz) cycle in an $Ar/CF_4/N_2$ discharge at $p = 30$ mTorr and applied voltage amplitude $V = 700$ V in the conventional cc rf reactor.

combination probability.[30] The cutoff parameter is chosen to be 1/5 of the mean electron velocity in each cell so that the probability that a randomly sampled electron has a velocity less than $(\nu_e)_{min}$ is only 1.1% in equilibrium.[30] If the number of the simulated electrons in a cell is N_e, the maximum number of the simulated electrons N_{re} that can recombine is calculated from[30]

$$(N_{re})_{max} = W_i \frac{N_e N_i}{V_c} \frac{a}{\sqrt{m_e/3e}} \frac{\Delta t}{(\nu_e)_{min}}. \quad (2)$$

The colliding electrons $(N_{re})_{max}$ are chosen randomly. Then it is checked for each electron with velocity ν_e whether it recombines with an ion, i.e., if a random number R is less than $(\nu_e)_{min}/\nu_e$. If $R \geq (\nu_e)_{min}/\nu_e$, the recombination is null.[30]

It should be kept in mind that in the case of different weights for ions W_i and electrons W_e, as in the present simulation, the maximum number of simulated ions that can recombine $(N_{ri})_{max}$ is not equal to $(N_{re})_{max}$ and is given by $(N_{ri})_{max} = (N_{re})_{max} W_e/W_i$.

For the electron – CF_3^+ recombination model, the ion temperature is determined as the mean energy in each cell, i.e., $T_i = m_i \langle \nu_i^2 \rangle / 3e$, where m_i and ν_i are the mass and velocity of the ion, respectively.[30]

In the simulation, the recombination time step is taken to be 10^5 times longer than the electron time step; the probability for recombination is, indeed, low because of the much lower ion densities in comparison with the neutral gas density.

III. RESULTS AND DISCUSSION

The calculations are performed for an $Ar/CF_4/N_2$ mixture at a ratio of 0.8/0.1/0.1. In Figs. 2-8, the rf powered electrode is at position 0 and the grounded electrode is at position 2 cm. The gas temperature is set to 300 K. The simulation grid is uniform and it consists of 100 cells. The electron time step is 3.7×10^{-11} s. To speed up the calculation, the ion time step is set to be 25 times longer than the electron time step. The choice of the grid spacing and the time steps is defined by the accuracy criteria for PIC/MC
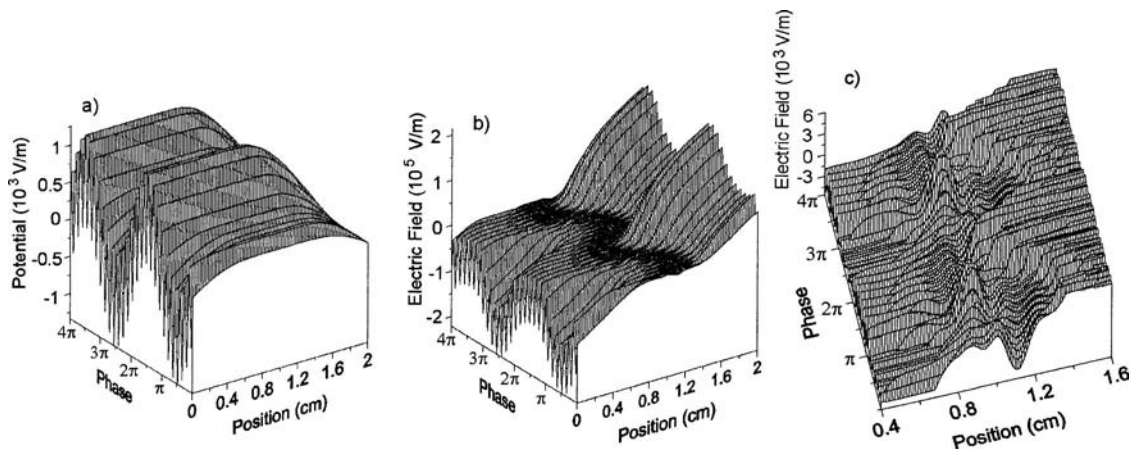
FIG. 3. Potential distribution (a) and electric-field distributions in the entire discharge (b), and in the bulk region (c), as a function of time in 2 LF (2 MHz) cycles in an $Ar/CF_4/N_2$ discharge at $p = 30$ mTorr and applied voltage amplitude $V = 700$ V in the dual-frequency (2 + 27 MHz) cc rf reactor.
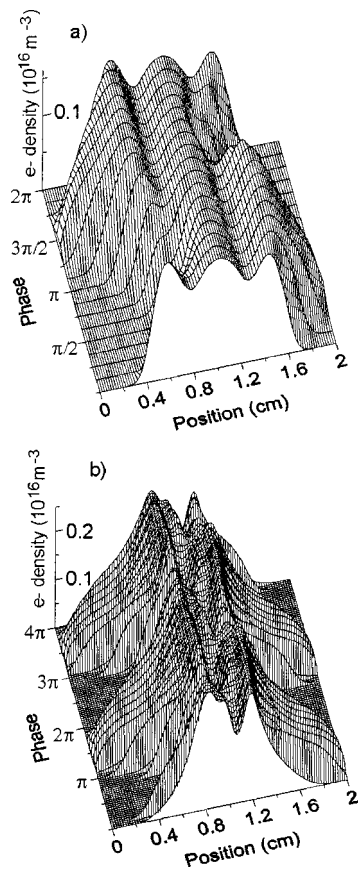
FIG. 4. Electron density distributions as a function of time in the rf cycle in the 13.56 MHz reactor (a) and as a function of time in two LF (2 MHz) cycles in the dual-frequency (2+27MHz) reactor (b). Applied voltage and pressure are the same as in Figs. 2 and 3, respectively.

codes with explicit mover.[15] Typical results of this model are electron and ion densities, fluxes and energy distributions, collision rates and electric field, and potential distributions. The calculated discharge quantities in the dual-frequency regime are saved at different phases in 2 LF and 27 HF cycles since one LF cycle does not contain an integer number of HF cycles. The discharge quantities in the single-frequency regime are saved at different phases in one cycle.

A. Potential and electric-field distributions

Figures 2 and 3 present the simulation results of the potential and electric-field distribution in the single- and dual-frequency regime, respectively. The results are given as a function of distance from the driven electrode and as a function of time in one HF (13.56 MHz) cycle in the conventional cc rf reactor, and in 2 LF (2 MHz) cycles in the dual-frequency (2+27 MHz) reactor. The behavior as a function of time and distance looks the same for both frequency regimes, but the difference is found in the absolute values. Indeed, the maximum and minimum values of the potential at the driven electrode in the dual-frequency regime are almost twice as large as those in the one-frequency regime, for the same applied voltage amplitude (700 V), and consequently, the electric field in the sheaths is also much stronger [cf. Figs. 2(a), 2(b), 3(a), and 3(b)].
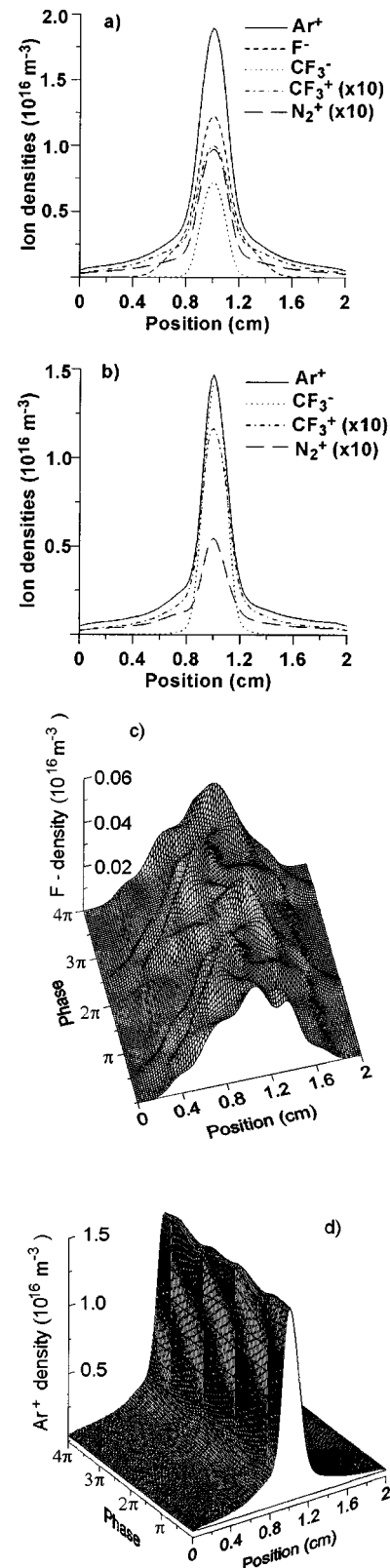

FIG. 5. Ion density distributions in the 13.56 MHz reactor (constant in time) (a) and at $\omega t = 0$ of the LF (2 MHz) cycle in the dual-frequency reactor (b). The F$^-$ ions and positive ions can respond to some extent to the LF. The F$^-$ and Ar$^+$ density distributions as a function of time in 2 LF cycles in the dual-frequency reactor are shown in (c) and (d). Applied voltage and pressure are the same as in Figs. 2 and 3, respectively.

The discharge structure is electronegative in both investigated schemes. A close look at the electric field in the bulk
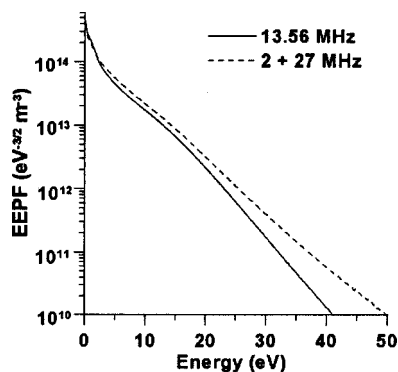
FIG. 6. EEPF in the center of the discharge averaged over one-HF cycle in the single-frequency reactor (solid line) and averaged over 2 LF cycles in the dual-frequency reactor (dashed line). Applied voltage and pressure are the same as in Figs. 2 and 3, respectively.

plasma [Figs. 2(c) and 3(c)] shows the appearance of double-layer structures (i.e., the local maxima or minima of the electric field) and field reversal near the bulk–sheath interface (cf. with the results for a pure CF_4 discharge, presented in Ref. 12). The electric field in the bulk plasma is substantial [up to 2000 V/m and 6000 V/m, Figs. 2(c) and 3(c), respectively] since the potential in the bulk is not constant in space. The sheaths are wide due to the narrow gap and the strong electric fields. The electric-field distribution is related to the charged particle density distributions.

B. Electron density distribution

The electron density distribution in both frequency regimes is shown in Fig. 4. In the single frequency reactor [Fig. 4(a)] the electrons move toward one of the electrodes depending on the phase of the applied voltage, i.e., toward the grounded electrode at phase $\pi/2$, and toward the powered electrode at phase $3\pi/2$. The electron density profile in the bulk is significantly different from the flat profile observed in computational and experimental investigations of an Ar/CF_4 discharge at 10% concentration of CF_4, applied voltage amplitude 200 or 240 V, and at a pressure range from 50 to 200 mTorr.[12,13] Indeed, peaks although not very prominent, appear at each bulk–sheath interface and in the bulk [Fig. 4(a)]. A low-energy group of electrons is formed, which pile up in
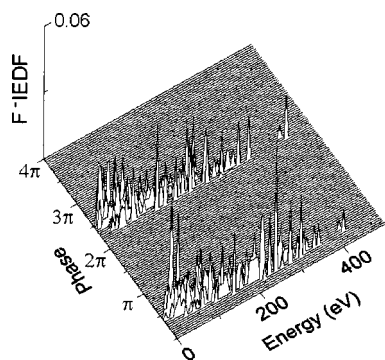

FIG. 7. Normalized F^- IEDF at the powered electrode as a function of time in 2 LF (2 MHz) cycles in a dual-frequency reactor. Applied voltage and pressure are the same as in Fig. 3.
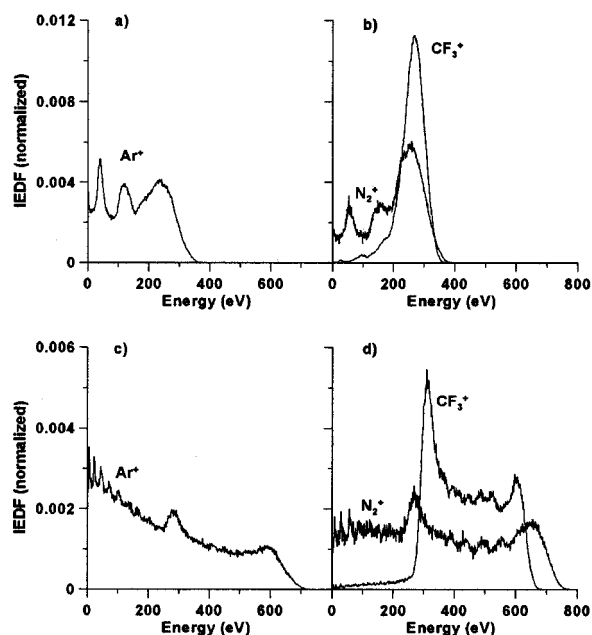

FIG. 8. Ar^+, CF_3^+, and N_2^+ IEDFs at the powered electrode, averaged over one-HF cycle in the conventional cc rf reactor [(a) and (b)], and averaged over 2 LF cycles in the dual-frequency reactor [(c) and (d)]. Applied voltage and pressure are the same as in Figs. 2 and 3, respectively.

the bulk plasma, because of the strong electric field and low pressure (i.e., low collision frequency).[32] This group can be detected in the electron energy probability function (EEPF) (see next). Its average energy is about 1.5 eV. Indeed, it is low, compared to the calculated averaged energy in the bulk, which has a value of about 6.5 eV. The peaks at each bulk–sheath interface are explained with the electron movement back and forth in the presence of negative ions.[12]

In the dual-frequency regime, the electron density and, consequently, the sheath width respond to the applied double frequency [Fig. 4(b)]. The electrons oscillate in one of the sheaths for a half LF (2 MHz) period with the applied HF (27 MHz). Two outstanding peaks and a secondary peak at the sheath–bulk interface are formed, which are related to the double-layer structures of the electric field [cf. Figs. 4(b) and 3(c)]. The electron density in the bulk plasma is calculated for both frequency regimes to be about $2 \times 10^{15}\,\mathrm{m}^{-3}$. This is lower than the density of the main negative ions by 1 order of magnitude (see next), i.e. the discharge structure is electronegative, both in the single- and dual-frequency regimes.

C. Ion density distributions

Figure 5 presents the ion density distributions for the single- and dual-frequency reactors. In the single-frequency reactor, the ion density profiles are constant in time throughout the HF cycle [Fig. 5(a)]. The dominant negatively charged species are negative ions, mainly F^- ($1.2 \times 10^{16}\,\mathrm{m}^{-3}$) and to a lesser extent CF_3^- ions ($6 \times 10^{15}\,\mathrm{m}^{-3}$). This is indeed clearly higher than the electron density. Since the diffusive flux of the negative ions is very low and the electric field is always directed outward, the negative ions are confined in the bulk plasma and are almost

absent in the sheath [Fig. 5(a)]. In the sheath, mainly positive ions and electrons are found [Figs. 5(a) and 4(a)]. The main positive ion is Ar^+ and its density in the bulk is $1.8 \times 10^{16} \, m^{-3}$. CF_3^+ and N_2^+ ions have densities, which are in the order of 1.0×10^{15} and $0.8 \times 10^{15} \, m^{-3}$, respectively, hence, more than an order of magnitude lower than the density of the Ar^+ ions.

For the dual-frequency reactor CF_3^- ions are the dominant negatively charged species with a density of $1.3 \times 10^{16} \, m^{-3}$ [Fig. 5(b)], whereas the density of the F^- ions is rather small, i.e., only $5 \times 10^{14} \, m^{-3}$ [Fig. 5(c)]. This is in contrast to investigations for cc single HF pure CF_4, Ar/CF_4, and $Ar/CF_4/N_2$ discharges (see Refs. 8–13). In the presence of LF (2MHz) and the high electric-field acceleration, the light F^- ions are not confined in the bulk plasma as in HF discharges. They have enough time to move toward the electrodes. The much heavier CF_3^- ions cannot respond to the LF and they remain in the bulk plasma [cf. Figs. 5(b) and 5(c)], where the only loss mechanism is the positive–negative ion recombination with extremely low reaction probability. This explains the higher CF_3^- density compared to the F^- density. The F^- density profile is greatly modulated by the LF and F^- ions are detected at the powered electrode at phase $\pi/2$ of the LF cycle [Fig. 5(c) and see next for the F^- ion energy distribution function (IEDF) at the powered electrode]. From the electric-field distribution, one could expect that F^- ions are able to reach the powered electrode at phase $3\pi/2$, when the electric field is almost 0, like the electrons [Figs. 3 and 4(b)]. However, at that time, F^- ions are detected at the grounded electrode [Fig. 5(c)]. Indeed, the F^- ions are inert in comparison with the electrons and 2 MHz is not low enough for F^- to respond instantaneously to the electric field. This explains the time delay (phase shift of half of a period, π). We have also carried out simulations for a dual-frequency $(1+27 \, MHz)$ reactor (not presented here), and they show that F^- ions reach the electrodes at a phase shifted with $\pi/2$ in comparison with the phase when the electric field is close to 0. Hence, a lower LF (1 MHz compared to 2 MHz) results in a smaller phase shift ($\pi/2$ versus π).

The positive ion density distributions, at phase 0 of the LF cycle in the dual-frequency reactor are presented in Fig. 5(b). The positive ions, can respond to the LF to some extent because the ion plasma frequency ω_{pi} (calculated to be $2.5 \times 10^7 \, s^{-1}$, $5.3 \times 10^6 \, s^{-1}$, and $5.8 \times 10^6 \, s^{-1}$ for Ar^+, CF_3^+, and N_2^+ ions, respectively) and the applied LF $\omega_{rf} = 1.3 \times 10^7 \, s^{-1}$ have comparable values. The main positive ion is again Ar^+ and its density in the bulk is $1.4 \times 10^{16} \, m^{-3}$. CF_3^+ and N_2^+ ions have densities of about 1.1×10^{15} and $0.6 \times 10^{15} \, m^{-3}$, respectively [Fig 5(b)]. The Ar^+ density as a function of time in two LF cycles is given in Fig. 5(d). The density profile depends on time although the dependence is weak.

D. Electron energy distribution

The main advantage of the PIC/MC method is that it does not require any assumption for the electron energy distribution function (EEDF), which is a crucial parameter in the discharge behavior. The EEDF is an output from the calculation. Figure 6 shows the EEPF $f_e(\varepsilon)$ $[=F_e(\varepsilon)\varepsilon^{-1/2}$, where $F_e(\varepsilon)$ is the EEDF and ε is the electron energy] at the center of the discharge and averaged for one HF cycle in the single-frequency reactor and for 2 LF cycles in the dual-frequency reactor. In the conventional HF reactor, the profile of the EEPF is complicated and can be approximated by a Maxwellian distribution in its low-energy part (i.e., until about 2 eV), and by a Druyvesteyn distribution in the higher-energy part (Fig. 6—solid line). A low-energy electron group is formed with average energy of 1.5 eV. The electron–neutral (mainly Ar because of the highest concentration in the gas mixture) collision frequency of this group ($\approx 7 \times 10^6 \, s^{-1}$) is smaller than the applied frequency ($\approx 9 \times 10^7 \, s^{-1}$), and the low-energy electrons oscillate without collisions in the bulk.[32]

In the dual-frequency reactor, the profile can be approximated by a bi-Maxwellian distribution (Fig. 6—dashed line). The two electron energy groups have energies of 3.5 and 7.5 eV. In the presence of the LF ($\omega_{LF} \approx 10^7 \, s^{-1}$), the two groups effectively interact with the neutrals. The calculated reaction rates show that all electron–neutral collisions in the dual-frequency regime have reaction rates from two to five times higher than the reaction rates in the single-frequency regime. The high-energy tails in both cases are due to the comparatively strong electric field in the bulk, which is a characteristic feature of electronegative discharges. The averaged electron energy determined by the EEDF is calculated to be 7.5 eV and 7.3 eV in the single- and dual-frequency regime, respectively.

E. Ion energy distributions

Figure 7 presents the normalized F^- IEDF at the driven electrode, where the wafer is placed in the dual-frequency reactor. Highly energetic F^- ions (with energy up to 400 eV) are detected at phase $\pi/2$ of the LF cycle [cf. also Fig. 5(c)]. The incident negative ion flux on the wafer reduces the local charging, which is an important issue in improving the performance of the anisotropic etching processes. The negative F^- ion injection was numerically observed also in an Ar/CF_4 discharge sustained in a pulsed two-frequency reactor during the off phase.[7] In the single-frequency reactor, the electron and positive ion fluxes on the wafer have the same magnitude for a short time during the anodic part of the rf cycle. During the cathodic part of the rf cycle, only positive ions reach the wafer. In the dual-frequency reactor, the electron flux on the wafer is substantial for a longer time during the anodic part of the LF cycle and is replaced by the negative F^- ion flux for a short time of the cathodic part of the LF cycle, reducing the accumulated charge in this way.

The Ar^+, CF_3^+, and N_2^+ IEDFs at the powered electrode, averaged over one HF cycle in the conventional cc rf reactor are presented in Figs. 8(a) and 8(b). The Ar^+, CF_3^+, and N_2^+ IEDFs at the powered electrode, averaged over 2 LF cycles in the dual-frequency reactor are presented in Figs. 8(c) and 8(d). The IEDFs in the single-frequency regime are narrow with one outstanding peak, whereas the IEDFs in the dual-

frequency regime are broad and bimodal as is expected in the presence of the LF.[33,34]

The parameter determining the shape of the IEDF is the relation τ_{ion}/τ_{rf}, where τ_{ion} is the ion transit time and $\tau_{rf} = 2\pi/\omega_{rf}$ is the rf period.[33]

In the HF regime, $\tau_{ion}/\tau_{rf} \gg 1$, i.e., the ions take many rf cycles to cross the sheath, and they respond only to the average sheath potential drop. In a collisionless sheath, this results in a narrow IEDF with one or two peaks, depending on the value of τ_{ion}/τ_{rf}.[33,34] The IEDF width ΔE is defined as $\Delta E = E_2 - E_1$, where E_1 and E_2 are the energies at which the peaks are observed. The width ΔE decreases with increasing τ_{ion}/τ_{rf} until, at some point, the two peaks can no longer be resolved. Analytical calculations and experiments in the HF regime show that the width ΔE is centered at $e\bar{V}_s$, where $\bar{V}_s$ is the mean sheath voltage drop, and it depends on the ion mass ($\Delta E \sim m_i^{-1/2}$).[33,34]

However, the sheaths in the etching reactors, at the conditions under study, cannot be considered collisionless. Elastic and charge exchange collisions broaden the IEDF profile and shift it toward lower energies. Charge exchange collisions lead to the formation of secondary peaks, which are placed at energies lower than E_1 and E_2.[33,34]

In the present simulation, for the single-frequency reactor, the two peaks coincide at energies lower than $e\bar{V}_s$ ($\bar{V}_s$ is calculated to be 282 V) [Figs. 8(a) and 8(b)]. The number of secondary peaks in the Ar^+ and N_2^+ IEDFs are due to the frequent resonant and nonresonant charge transfer collisions between Ar^+ or N_2^+ and Ar or N_2. The charge transfer reaction, $CF_3^+ - CF_3$, is not considered in the model since the density of the CF_3 radicals is much lower in comparison with the CF_4 density, with a value in the order of $10^{18} m^{-3}$.[9,10] The elastic collisions $CF_3^+ - CF_4$ shift the position of the primary peak to an energy of 270 eV (cf. with the calculated $\bar{V}_s$ above). The Ar^+ and N_2^+ peaks are placed at energies of 240 eV and 260 eV, respectively, due to the influence of both types of collisions. The dependence on the ion mass is also observed. Indeed, the heaviest CF_3^+ ion has a narrow IEDF maximum compared to the wider Ar^+ and N_2^+ primary peaks.

In the LF regime, the ion transit time τ_{ion} is less than the rf period τ_{rf}, i.e., the ions cross the sheath in a small fraction of the rf cycle and they reach the electrode with an energy equal to the instantaneous sheath potential drop.[33,34] In this simulation τ_{ion}/τ_{LF}, where τ_{LF} is the LF period ($f = 2$ MHz), is calculated to be 0.9, 1.2, and 0.7 for Ar^+, CF_3^+, and N_2^+ ions, respectively. The two outstanding peaks in the profile correspond to the averaged minimum and maximum sheath potential drop. In collisionless LF sheaths, the distribution is independent of the ion mass.[33] However, in the present dual-frequency regime, the influence of the applied HF (27 MHz) is observed and the IEDF width depends on the ion mass m_i, i.e., as m_i is increased, ΔE is reduced [cf. the IEDF width for the three positive ions in Figs. 8(c) and 8(d), considering that $m_{N_2+} < m_{Ar+} < m_{CF_3+}$]. The influence of the collisions is the same as in the single-HF regime.

IV. SUMMARY

A one-dimensional PIC/MC model has been developed to describe the structure of a cc rf discharge in a gas mixture of Ar, CF_4, and N_2. The model follows electrons, Ar^+, CF_3^+, F^-, CF_3^-, and N_2^+ ions. The collisions treated by the MC method include electron–neutral (Ar, CF_4, and N_2) collisions, various kinds of collisions of Ar^+, CF_3^+, F^-, CF_3^-, or N_2^+ with neutrals, positive–negative ion recombination, and electron–ion recombination.

The simulations are performed for 0.8/0.1/0.1 ratios of Ar/CF_4/N_2 mixture at a pressure of 30 mTorr in single- (13.56 MHz) and dual-frequency ($2 + 27$ MHz) cc reactors and a comparison between the two frequency regimes is made. The model yields results for the electron and various ion densities, their fluxes and energy distributions, the collision rates and the electric field, and potential distributions. The results are presented as a function of distance to the driven electrode and as function of time in one HF cycle in the single-frequency reactor, and in two LF cycles in the dual-frequency reactor.

The results show that the structure of the discharge is electronegative in both investigated regimes, i.e. double-layer structure and electron density maxima at the bulk–sheath interface are observed, and the main negative carriers are the negative ions. The electron densities in the bulk have similar values in the two regimes. In the dual-frequency regime, the electrons oscillate in one of the sheaths for half of a LF (2 MHz) period with the applied HF (27 MHz). The main negative ion in the single-frequency regime is F^-, whereas it is CF_3^- in the dual-frequency regime. Indeed, in the presence of LF (2 MHz) and the strong electric-field acceleration, the light F^- ions are not confined in the bulk plasma as in single-HF discharges and they have enough time to move toward the electrodes. Highly energetic F^- ions (with energy up to 400 eV) are detected at phase $\pi/2$ of the LF cycle at the driven electrode and at phase $3\pi/2$ of the LF cycle at the grounded electrode. The much heavier CF_3^- ions cannot respond to the LF and they remain in the bulk plasma. The positive ion densities do not depend on the phase in the single-frequency reactor. However, in the dual-frequency reactor, the positive ions respond slightly to the LF. The main positive ion is Ar^+. The densities of each of the positive ions have similar values in the two regimes.

The calculated EEPF profiles can be approximated to a Druyvesteyn and bi-Maxwellian distribution with high-energy tails in the single- and dual-frequency regime, respectively. The IEDF in the single-frequency regime is narrow with one outstanding peak, whereas the IEDF in the dual-frequency regime is broad and bimodal. The IEDF energy width depends on the ion mass.

In conclusion, the present simulations show that the dual-frequency regime improves the following plasma parameters, which are very important in the etching processes:

(1) It provides a significantly wider ion bombardment energy range in comparison with the single-HF configuration.

(2) It reduces the charge accumulation by F^- injection to the electrodes.

(3) It randomizes the electron energy by a higher electron–neutral collision frequency in comparison with the single-HF regime at the same pressure. This results in an EEDF distribution, close to the bi-Maxwellian, which can significantly simplify further calculations of plasma quantities determined by the EEDF.

ACKNOWLEDGMENTS

[1] H. H. Goto, H.-D. Löwe, and T. Ohmi, J. Vac. Sci. Technol. A **10**, 3048 (1992); H. H. Goto, H.-D. Löwe, and T. Ohmi, IEEE Trans. Semicond. Manuf. **6**, 58 (1993).

[2] W. Tsai, G. Mueller, R. Lindquist, B. Frazier, and V. Vahedi, J. Vac. Sci. Technol. B **14**, 3276 (1996).

[3] V. Vahedi and G. DiPeso, J. Comput. Phys. **131**, 149 (1997).

[4] H. C. Kim and V. I. Manousiouthakis, J. Vac. Sci. Technol. A **16**, 2162 (1998).

[5] T. Kitajima, Y. Takeo, and T. Makabe, J. Vac. Sci. Technol. A **17**, 2510 (1999); T. Kitajima, Y. Takeo, Z. L. Petrović, and T. Makabe, Appl. Phys. Lett. **77**, 489 (2000).

[6] S. Rauf and M. J. Kushner, IEEE Trans. Plasma Sci. **27**, 1329 (1999).

[7] K. Maeshige, G. Washio, T. Yagisawa, and T. Makabe, J. Appl. Phys. **91**, 9494 (2002).

[8] M. Haverlag, A. Kono, D. Passchier, G. M. W. Kroesen, W. J. Goedheer, and F. J. de Hoog, J. Appl. Phys. **70**, 3472 (1991); J. L. Jauberteau, G. J. Meeusen, M. Haverlag, G. M. W. Kroesen, and F. J. de Hoog, J. Phys. D **24**, 261 (1990).

[9] N. V. Mantzaris, A. Boudouvis and E. Gogolides, J. Appl. Phys. **77**, 6169 (1995); E. Gogolides, M. Stathakopoulos, and A. Boudouvis, J. Phys. D **27**, 1878 (1994).

[10] J. P. Booth, G. Cunge, P. Chabert, and N. Sadeghi, J. Appl. Phys. **85**, 3097 (1999).

[11] K. Denpoh and K. Nanbu, J. Vac. Sci. Technol. A **16**, 1201 (1998).

[12] V. Georgieva, A. Bogaerts, and R. Gijbels, J. Appl. Phys. **93**, 2369 (2003).

[13] K. Kaga, T. Kimura, T. Imaeda and K. Ohe, Jpn. J. Appl. Phys., Part 1 **40**, 6115 (2001).

[14] C. K. Birdsall and A. B. Langdon, *Plasma Physics via Computer Simulation* (McGraw–Hill, New York, 1985).

[15] E. Kawamura, C. K. Birdsall, and V. Vahedi, Plasma Sources Sci. Technol. **9**, 413 (2000).

[16] P. Belenguer and J. P. Boeuf, Phys. Rev. A **41**, 4447 (1990).

[17] M. Surendra and D. B. Graves, IEEE Trans. Plasma Sci. **19**, 144 (1991).

[18] B. Chapman, *Glow Discharge Processes* (Wiley, New York, 1980).

[19] V. Vahedi and M. Surendra, Comput. Phys. Commun. **87**, 179 (1995).

[20] A. Okhrimovskyy, A. Bogaerts, and R. Gijbels, Phys. Rev. E **65**, 037402 (2002).

[21] K. Nanbu and K. Denpoh, J. Phys. Soc. Jpn. **67**, 1288 (1998).

[22] A. V. Phelps and Z. L. Petrovic, Plasma Sources Sci. Technol. **8**, R21 (1999).

[23] A. V. Phelps and L. C. Pitchford, Phys. Rev. A **31**, 2932 (1985); A. V. Phelps *et al.*, Joint Institute for Laboratory Astrophysics (JILA) Information Center Report No. 26 (1985), to be found on ftp://jila.colorado.edu/collision_data

[24] M. Kurihara, Z. Lj. Petrovic, and T. Makabe, J. Phys. D **33**, 2146 (2000).

[25] R. A. Bonham, Jpn. J. Appl. Phys., Part 1 **33**, 4157 (1994).

[26] F. Debal, J. Bretagne, M. Jumet, M. Wautelet, J. P. Dauchot, and M. Hecq, Plasma Sources Sci. Technol. **7**, 219 (1998).

[27] A. V. Phelps, J. Phys. Chem. Ref. Data **20**, 557 (1991); A. V. Phelps, J. Appl. Phys. **76**, 747 (1994).

[28] M. R. Spalburg and E. A. Gislason, Chem. Phys. **94**, 339 (1985).

[29] S. Rauf and M. J. Kushner, J. Appl. Phys. **82**, 2805 (1997).

[30] K. Denpoh and K. Nanbu, Jpn. J. Appl. Phys., Part 1 **39**, 2804 (2000).

[31] J. Henriques, E. Tatarova, V. Guerra, and C. M. Ferreira, J. Appl. Phys. **91**, 5622 (2002).

[32] V. A. Godyak and R. B. Piejak, Phys. Rev. Lett. **65**, 996 (1990).

[33] E. Kawamura, V. Vahedi, M. A. Lieberman, and C. K. Birdsall, Plasma Sources Sci. Technol. **8**, R45 (1999).

[34] W. J. Goedheer, Plasma Sources Sci. Technol. **9**, 507 (2000).